





Article

# Composition of Sedimentary Organic Matter across the Laptev Sea Shelf: Evidences from Rock-Eval Parameters and Molecular Indicators

Elena Gershelis <sup>1,\*</sup>, Andrey Grinko <sup>1</sup>, Irina Oberemok <sup>1</sup>, Elizaveta Klevantseva <sup>1</sup>,  
Natalina Poltavskaya <sup>1</sup>, Alexey Ruban <sup>1</sup>, Denis Chernykh <sup>2</sup>, Andrey Leonov <sup>3</sup>,  
Natalia Guseva <sup>1</sup> and Igor Semiletov <sup>1,2</sup>

<sup>1</sup> School of Earth Sciences and Engineering, Tomsk Polytechnic University, 634050 Tomsk, Russia; grinko@tpu.ru (A.G.); genuine.i@yandex.ru (I.O.); eklevantceva@mail.ru (E.K.); geo.ikigai@yandex.ru (N.P.); ruban@tpu.ru (A.R.); gusevanv@tpu.ru (N.G.); ipsemiletov@alaska.edu (I.S.)

<sup>2</sup> Pacific Oceanological Institute, Far East Branch of Russian Academy of Sciences, 690041 Vladivostok, Russia; denis.chernykh.vl@gmail.com

<sup>3</sup> Engineering School of New Manufacturing Technologies, Tomsk Polytechnic University, 634050 Tomsk, Russia; laa91@tpu.ru

\* Correspondence: elenapanova@tpu.ru

Received: 16 November 2020; Accepted: 8 December 2020; Published: 14 December 2020



**Abstract:** Global warming in high latitudes causes destabilization of vulnerable permafrost deposits followed by massive thaw-release of organic carbon. Permafrost-derived carbon may be buried in the nearshore sediments, transported towards the deeper basins or degraded into the greenhouse gases, potentially initiating a positive feedback to climate change. In the present study, we aim to identify the sources, distribution and degradation state of organic matter (OM) stored in the surface sediments of the Laptev Sea (LS), which receives a large input of terrestrial carbon from both Lena River discharge and intense coastal erosion. We applied a suite of geochemical indicators including the Rock Eval parameters, traditionally used for the matured OM characterization, and terrestrial lipid biomarkers. In addition, we analyzed a comprehensive grain size data in order to assess hydrodynamic sedimentation regime across the LS shelf. Rock-Eval (RE) data characterize LS sedimentary OM with generally low hydrogen index (100–200 mg HC/g TOC) and oxygen index (200 and 300 CO<sub>2</sub>/g TOC) both increasing off to the continental slope. According to T<sub>peak</sub> values, there is a clear regional distinction between two groups (369–401 °C for the inner and mid shelf; 451–464 °C for the outer shelf). We suggest that permafrost-derived OM is traced across the shallow and mid depths with high T<sub>peak</sub> and slightly elevated HI values if compared to other Arctic continental margins. Molecular-based degradation indicators show a trend to more degraded terrestrial OC with increasing distance from the coast corroborating with RE results. However, we observed much less variation of the degradation markers down to the deeper sampling horizons, which supports the notion that the most active OM degradation in LS land-shelf system takes part during the cross-shelf transport, not while getting buried deeper.

**Keywords:** organic carbon; biomarkers; Rock-Eval pyrolysis; grain size; permafrost; surface sediments; Laptev Sea

## 1. Introduction

The interactions between climate and global carbon cycle in the Arctic region are undergoing substantial changes due to degradation of the vulnerable permafrost carbon pool. Arctic permafrost region holds the large pool of soil organic carbon (1300 PgC) including 800 PgC as perennially frozen [1],

meanwhile carbon stocks in subsea permafrost are estimated at around 1400 PgC [2,3]. This permafrost pool destabilization followed by a massive thaw-release of organic carbon triggers many complex biogeochemical mechanisms including intensive mobilization and increasing supply of terrigenous organic carbon (OC) due to coastal erosion and riverine runoff to the coastal ocean [3–6]. First studies of biogeochemical consequences of coastal erosion in the Arctic ocean were initiated in the 1990s by discovery of anomalous high values of carbon dioxide (CO<sub>2</sub>) in terms of CO<sub>2</sub> partial pressure, pCO<sub>2</sub> [7,8]. It has been found that rapid oxidation of eroded carbon is the main reason for CO<sub>2</sub> evasion and extreme acidification in the Arctic seas [9,10]. Therefore, the fate of terrigenous OC after it is translocated to the Arctic Ocean has been the subject of growing scientific interest in recent years [11–13].

The East Siberian Arctic shelf (ESAS), the world's largest continental shelf, receives substantial input of terrigenous OC both through enhancing discharge of Great Russian Rivers, which drain the vast Siberian permafrost areas, and from intensive erosion of coastal organic-rich Pleistocene-age permafrost (Yedoma). Previous studies on this region have demonstrated that different sources and contrasting composition of terrigenous OC may affect its transportation, accumulation and degradation patterns. These patterns were traced both for particulate OC and sedimentary OC by a suite of biogeochemical parameters, including molecular markers composition, isotopic fingerprints ( $\Delta^{14}\text{C}$ ,  $\delta^{13}\text{C}$ ) [3,12,14–18] and sedimentological characteristics [14,19,20].

An additional informative geochemical method, Rock-Eval (RE) pyrolysis, was traditionally used in petroleum geochemistry to assess the hydrocarbon potential of the source rocks at the exploration stage [21–26]. In the recent decades, this method has been increasingly applied to study recent organic matter stored in freshwater and marine surface sediments, peat and soils [27–34]. These studies showed that RE results may significantly contribute to identification of the OM sources, distribution and degradation state. Along with widely used molecular and isotopic proxies, RE data complement and extend geochemical interpretation of the OM nature. However, there is a lack of RE studies performed for the modern OM across the Arctic seas. Thus, Hare and coauthors performed an extensive investigation of recent sediment cores from the Hudson Bay and demonstrated an ability of RE parameters to provide an indication of the OM preservation/degradation state and resolve its biogeochemical nature [28]. RE results obtained for the Arctic seas sediments were also reported in [35–38] and several other studies. Along with other geochemical tools RE pyrolysis was also applied by [39,40] in order to assess past microbial activity and quality of coastal permafrost OM from different depositional ages with regard to its biodegradability and greenhouse gas production from thawing deposits.

In this study, we investigate the sources and distribution of the OM accumulated in the surface sediments across the Laptev Sea shelf from the coastal zone to the offshore areas. We characterized the sediments using RE indicators along with traditional molecular markers (n-alkanes; n-alkanoic acids). Besides, we provide a detailed grain size composition of sediments to characterize hydrodynamic regimes acting across the Laptev Sea (LS) margin.

## 2. Materials and Methods

### 2.1. Study Area

The LS, the shallowest sea in the Arctic Ocean, covers almost 500,000 km<sup>2</sup> and is characterized by a mean depth of less than 50 m [41]. The main part of OC for the LS originates from terrestrial sources comprising river discharge and a coastal erosion input while marine production is generally low due to low light and nutrient limited conditions [36,42]. The destabilization of Pleistocene Ice Complex deposits (ICD) is believed to be a major contributor to the OC pool along the Siberian coastline [3] and to the LS waters [43]. The Lena River is the main contributor of dissolved OM, while the main portion of suspended riverine OM is settled down in the river-sea mixing zone [44].

The drained watershed of Lena River is about  $2.46 \times 10^6$  km<sup>2</sup>, where 90% is underlain by continuous and discontinuous permafrost [45].

Sediment transport mechanisms are heavily affected by seasonal factors. Ice cover lasting 8–9 months per year blocks wind-forced water mass mixing and, thereby, eliminates sediment resuspension and suppresses sedimentation processes within the land–sea system. Eventually, this environment not only forms a gently dipping underwater plain but also promotes accumulation of fine-grained sediments, atypical for shallow coastal areas [46]. Sedimentation in short ice-free period is strongly influenced by wind and wave action and characterized by increasing river discharge. During and shortly after the river-ice breakup (June–early July) sediment plume intrudes into the eastern shelf within the surface layer beneath the fast ice, then sinks into the bottom nepheloid layer on the mid-shelf and goes back to the inner shelf where it could ultimately be incorporated into newly formed ice and transferred with the ice into outer shelf and further [47]. Wave-driven sediments mobilization generally refers to the polynya where fine-grained bottom material is being resuspended during turbulence and transported offshore [48,49].

## 2.2. Sampling

Sampling area covers a representative transect from close to the Lena delta to the continental slope of the Laptev Sea with different water depths ranging from 14.5 along the coastline (station 6005) to 375 m on the outer shelf (station 6527; Figure 1). Surface sediments were collected during complex research expeditions onboard the R/V “Academician M. V. Keldysh” in September–October 2018–2019. The samples were taken at 21 stations with a box-corer. Once recovered, samples were subsampled and sectioned into 0–2 cm, 2–5 cm and 5–10 cm intervals within the upper 10 cm of the sediment cores with sediments from individual horizons placed in sealed containers and stored frozen at  $-18$  °C until further analyses. In the laboratory, samples were thawed for 24 h at room temperature and oven-dried at  $40$  °C to constant weight. Prior to analyses, a subsample from each surface sample was homogenized.

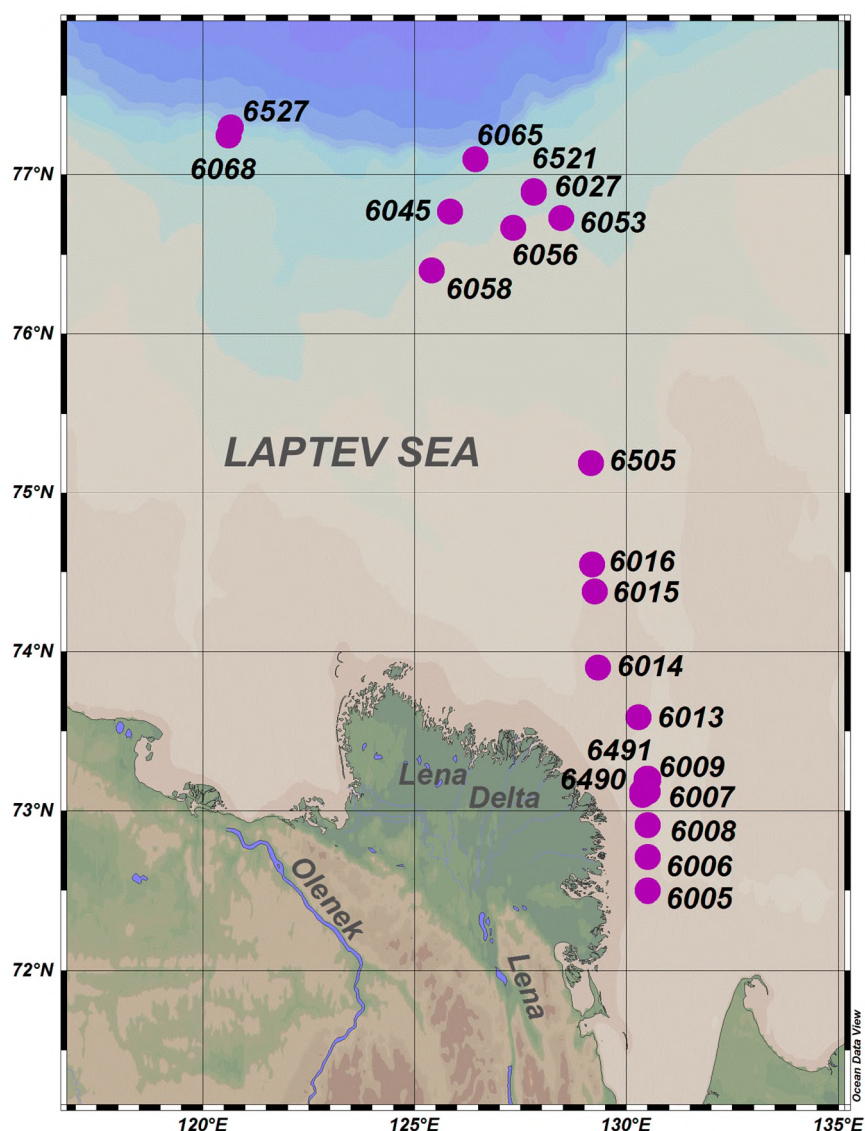


**Figure 1.** Study area in the Laptev Sea. Pink filled circles mark the sediment sampling sites.

### 2.3. Analytical Methods

Grain size measurements were performed using a Shimadzu SALD-7101 laser particle size analyzer. Analyses were performed at least five times on each sample, the mean values of each parameter were calculated and the associated standard deviations were  $< 3\%$ .

The measured particle size spectrum was presented as % volume in a logarithmic scale, where volume was calculated from particle diameter, assuming spherical shapes. Results were recalculated to fractions of clay ( $< 2 \mu\text{m}$ ), fine silt ( $2\text{--}10 \mu\text{m}$ ), sortable silt ( $10\text{--}63 \mu\text{m}$ ) and sand ( $> 63 \mu\text{m}$ ). We calculated mean grain size ( $M_z$ ), standard deviation ( $\sigma$ ), skewness ( $S_k$ ) and kurtosis ( $K_G$ ) as described in [50]. Considering its statistical reliability, we also used median grain size ( $M_d$ ) to describe particle size distribution properly.

Pyrolytic analyses were performed on a Rock-Eval 6 Turbo (Vinci Technologies) at the Arctic Carbon Laboratory, Tomsk polytechnic university, according to the pyrolysis program for the recent OM analysis proposed by [51]. Rock-Eval (RE) pyrolysis is a two-step process combining pyrolysis in an oxygen-free atmosphere and combustion under oxic conditions. The procedure started at  $180 \text{ }^\circ\text{C}$  with a heating rate of  $25 \text{ }^\circ\text{C}/\text{min}$  to release S1 fraction (mg HC/g) representing volatile compounds. This phase was followed by heating until  $650 \text{ }^\circ\text{C}$  to yield S2 fraction (mg HC/g) largely indicating a

breakdown of complex molecules [52]. The released hydrocarbons were measured by a flame ionization detector. The amounts of CO and CO<sub>2</sub> representing the S3CO (mg CO/g) and S3 (mg CO<sub>2</sub>/g) peaks, respectively, were measured continuously by an infrared detector during a pyrolysis step. The sample was then combusted in an oxidation chamber heating to 850 °C with a heating rate of 20 °C/min. This additional oxidation step produced residual organic carbon (RC) and inorganic carbon (MinC) values (in wt %). The total organic carbon content was calculated as a sum of pyrolyzed and residual fractions. Hydrogen index (HI) and oxygen index (OI) are determined from the ratios of S2/TOC and S3/TOC, respectively. Surface sediments were analyzed for lipid biomarkers as described earlier in [6]. Briefly, homogenized sediments were extracted in dichloromethane:methanol (DCM:MeOH 2:1 v/v) using the Soxhlet apparatus for 24 h. Total lipid extracts (TLE) were concentrated to 2 mL using rotary evaporation and purified by adding activated copper for sulfur removal and anhydrous Na<sup>2</sup>SO<sub>4</sub> for water removal. TLE were separated into hydrocarbon, polar and acid fractions using Bond-Elut column chromatography. We also conducted a series of blank experiments to identify and account for contaminants. In this study, we only reported data for n-alkanes and n-alkanoic acids. Quantification and recoveries were controlled with commercially available internal standards (D50-tetracosane and D39-eicosanoic acid).

All fractions were analyzed separately by chromatography–mass spectrometry (GC–MS) on a Agilent 7890B (GC)—Agilent Q-TOF 7200 (MS) instrument using HP-1MS quartz capillary column (length 30 m, internal diameter 0.25 mm and film thickness 0.25 μm) with secondary ionization in the collision cell with nitrogen as a collision gas at a collision energy of 10 eV. A temperature profile was initially started at 40 °C followed by a ramp of 5 °C min<sup>-1</sup> until reaching 150 °C and then by a ramp of 3 °C min<sup>-1</sup> until reaching and holding at 310 °C for 20 min. Carrier gas (helium) speed was 1.1 mL/min and injection volume was 1 μL. Measurements were carried out both in scan (*m/z* range 50–500) and selected ion monitoring (SIM) modes at 70 eV. Components identification was performed using NIST 14 library and with a detailed study of the mass spectra of fragment and molecular ions using previously published data.

### 3. Results and Discussion

#### 3.1. Grain Size Distribution along the Studied Profile

Table 1 provides the detailed grain-size characteristics of the Laptev Sea surface sediments. Overall, the sediments along the studied profile were predominantly composed of sortable (20.2–67.6%, average 48.0%) and fine silt (11–41.1%, average 28.8%) with certain proportions of the clay (9.1–39.9%, average 18.3%) and sand (0–51.8%, average 5.0%) fractions. The skewness range, kurtosis values and sorting coefficient were −0.59–0.53, 0.71–1.937 and 3.05–14.18 with average values of −0.3, 1.3 and 4.8, respectively.

**Table 1.** Grain size characteristics.

Station	Sampling Horizon	Lat °N	Long °E	Depth, m	Grain Size Classes. %				Grain Size Parameters				
					Sand (>63 µm)	Sortable Silt (63–10 µm)	Fine Silt (10–2 µm)	Clay (<2 µm)	M <sub>d</sub> , µm <sup>a</sup>	M <sub>z</sub> , µm <sup>a</sup>	Sk <sup>b</sup>	K <sub>G</sub> <sup>c</sup>	σ <sup>d</sup>
6005	0–2	72.5	130.5	14.5	51.8	28.1	11.0	9.1	99.69	52.84	−0.589	0.891	6.817
	2–5				0.0	66.3	24.5	9.2	11.11	10.02	−0.313	1.515	3.143
6006	0–2	72.71	130.5	18.5	0.1	48.1	21.2	30.6	8.527	7.849	−0.394	1.923	3.871
	2–5				0.1	67.4	22.0	10.5	11.28	10.01	−0.357	1.677	3.052
6007	0–2	73.12	130.5	24.3	0.0	47.6	31.7	20.7	9.418	8.297	−0.369	1.521	3.608
	2–5				0.1	52.5	33.6	13.7	8.254	7.006	−0.325	1.443	3.214
6008	0–2	72.91	130.5	22	0.0	41.2	32.0	26.8	7.368	6.987	−0.401	1.937	3.993
	2–5				0.0	62.6	24.0	13.4	11.68	10.118	−0.373	1.572	3.114
6009	0–2	73.12	130.37	24	0.0	46.9	24.6	28.5	9.638	8.119	−0.303	1.734	3.243
	2–5				0.1	67.6	22.6	9.7	10.25	8.800	−0.364	1.579	3.161
6013	0–2	73.59	130.28	23.5	0.0	52.8	24.1	23.1	8.647	6.294	−0.550	1.147	3.908
	2–5				0.0	36.0	35.3	28.7	4.819	2.758	−0.546	1.032	7.487
6014	0–2	73.9	129.32	40	100	0.0	0.0	0.0	267.1	299.6	0.499	2.280	1.489
6015	0–2	74.38	129.25	64	100	0.0	0.0	0.0	210.8	213.6	0.253	1.391	1.395
6016	2–5	74.55	129.18	72	0.0	54.4	34.0	11.6	8.738	7.602	−0.313	1.189	3.175
6027	0–2	76.9	127.8	65	0.0	54.9	29.1	16.0	8.794	6.876	−0.393	1.268	3.443
	2–5				0.0	55.5	30.9	13.6	9.084	7.590	−0.352	1.184	3.416
6045	0–2	76.77	125.83	72	1.2	54.9	31.8	12.1	9.175	8.222	−0.231	1.288	3.564
	2–5				0.0	44.7	39.8	15.5	6.826	5.871	−0.329	1.229	3.110
6053	0–2	76.73	128.45	65	0.4	55.1	28.5	16.0	8.952	6.998	−0.384	1.263	3.509
	2–5				0.0	40.9	36.1	23.0	5.678	3.469	−0.530	1.621	6.099
6056	0–2	76.67	125.47	62	0.2	41.6	29.4	28.8	5.650	2.865	−0.430	0.706	6.818
	2–5				0.0	37.3	31.4	31.3	4.75	2.494	−0.516	0.858	7.486
6058	0–2	76.4	126.42	52	7.7	48.2	31.8	12.3	9.198	9.491	−0.079	1.251	4.322
	2–5				0.0	40.4	41.1	18.5	5.693	4.650	−0.356	1.236	3.412
6065	0–2	77.1	126.43	251	2.4	60.8	21.3	15.5	12.33	9.514	−0.397	1.371	4.906
	2–5				3.2	43.9	41.1	11.8	7.312	6.769	−0.131	1.397	3.312
6068	0–2	77.25	120.37	185	0.0	58.8	26.0	15.2	9.540	7.782	−0.350	1.340	3.595
	2–5				11.1	20.5	28.5	39.9	3.441	2.014	−0.226	0.815	12.08
6490	0–5	73.1	130.37	21	15.7	56.3	14.6	13.4	14.42	14.57	−0.161	1.280	4.768
	5–10				0.9	43.9	40.6	14.6	6.853	6.305	−0.166	1.392	3.455
6491	0–5	73.11	130.38	24	13.9	54.0	18.4	13.7	12.10	12.76	−0.110	1.352	4.840
6505	0–5	75.19	129.14	40	13.5	44.6	28.7	13.2	9.932	11.08	−0.044	1.036	5.012
	5–10				20.5	20.2	30.1	29.2	5.313	4.049	−0.180	0.709	14.18
6521	0–5	76.89	127.81	65	15.2	44.9	26.9	13.0	10.52	11.64	−0.057	0.985	5.097
6527	0–5	77.3	120.66	375	10.3	38.5	31.4	19.8	6.52	5.96	0.273	1.230	4.093

<sup>a</sup> M<sub>d</sub>—median grain size; M<sub>z</sub>—mean grain size; <sup>b</sup> Sk—skewness; <sup>c</sup> K<sub>G</sub>—kurtosis; <sup>d</sup> σ—standard deviation. Basic grain size characteristics without calculated statistics for the horizon 0–2 cm have been reported earlier in [53].

Particle size distribution and grain size statistics are in line with previously published data from the Laptev Sea shelf [46,54,55]. In the present study, we observe overall prevailing of fine-grained (<63  $\mu\text{m}$ ) surface sediments that can be explained by stable subglacial sedimentation environment, i.e., gravitational settling of suspended particles beyond the reach of any wave action. We also observed two samples from the mid-shelf (stations 6014 and 6015; sampling horizon 0–2 cm) with 100% sand content; these specific data were not included in the statistics calculated for this study. The outer shelf sediments also contain slightly elevated average sand fraction indicating an active hydrodynamic factors.

Our findings point to several external factors that may explain local accumulation of very poorly sorted coarse-grained surface sediments on the mid and outer shelves. Firstly, Shakhova and coauthors [56,57] have documented numerous gas flows at these depths escaping from the seafloor as bubble streams and presumably removing the fine-grained fraction from the surface deposits. Secondly, geophysical observations have repeatedly detected the ice scours both in the coastal zone, and on the outer part of ESAS [58–61]. Age of these scours is still under debate [62,63]. Jakobsson and coauthors provide evidence of a kilometer-thick ice shelf covering the entire central Arctic Ocean and extending up to present-day New Siberian Islands during the glacial maximum (Marine Isotope Stage 6, 140 ka BP) [62]. Moreover, another study reported on a glacially excavated trough discovered on the ESAS (De Long Trough), which is also dated to Marine Isotope Stage 6 [64]. However, it seems reasonable to assume the modern exaration processes considering the sedimentation rates (from 0.12 to 1.3  $\text{mm year}^{-1}$ ) estimated for this region in previous studies [11,65]. Recent ice scouring may explain the freshly exposed coarse-grained sediments, not yet overlain or thinly covered with fine-grained deposits. Nevertheless, modern ice-scouring process can hardly affect the outer shelf sediments at >200 m depth. Furthermore, coarse-grained sediments can be exported from eroding Siberian Yedoma Ice Complex coastlines [66–68] or rather transported via lateral brine injections produced by bottom dense-water eddies [69].

### 3.2. Sedimentary OM Composition on the Bulk Level from RE Pyrolysis

TOC concentrations decreased with increasing distance from the coastline with the highest values (>2.5%) at shallow coastal areas and lowest values on the outer shelf (0.5%; Table 2). TOC values were in accordance with the data reported by previous researchers [11,55,58,65]. Pyrolyzable carbon (PC) composed from 20 to 30% of the TOC ( $r^2 = 0.82$ ). The most thermo-labile fractions of PC (S1 and S2) were strongly correlated ( $r^2 = 0.72$ ) with S2 values on average 4 times higher than S1. S3 was highly correlated with S2 ( $r^2 = 0.83$ ) and weakly correlated with S1 ( $r^2 \sim 0.4$ ).

**Table 2.** Rock-Eval parameters of the Laptev Sea (LS) surface sediments.

Station	Sampling Horizon	T <sub>peak</sub> , °C <sup>a</sup>	S1 <sup>b</sup> , mgHC/TOC	S2 <sup>b</sup> , mgHC/TOC	S3 <sup>b</sup> , mgCO <sub>2</sub> /TOC	PC <sup>c</sup> , %	RC <sup>c</sup> , %	TOC <sup>c</sup> , %	HI <sup>d</sup>	OI <sup>d</sup>	MinC <sup>c</sup> , %
6005	0–2	461	0.37	1.78	3.02	0.28	1.14	1.42	125	213	0.2
	2–5	461	0.38	1.52	2.74	0.26	1.13	1.39	109	197	0.23
6006	0–2	462	0.65	2.92	5.74	0.5	2.21	2.71	108	212	0.4
	2–5	463	0.8	3.35	4.8	0.52	2.04	2.56	131	188	0.31
6007	0–2	462	0.73	2.74	5.32	0.64	2.01	2.65	103	201	0.4
	2–5	463	0.84	2.9	4.77	0.49	1.96	2.45	118	195	0.34
6008	0–2	462	0.71	2.61	4.82	0.48	1.79	2.27	115	212	0.3
	2–5	464	0.65	2.4	4.47	0.41	1.75	2.16	111	207	0.36
6009	0–2	461	0.53	1.98	3.84	0.35	1.58	1.93	103	199	0.3
	2–5	462	0.53	2.06	3.88	0.35	1.54	1.89	109	205	0.33
6013	0–2	464	0.28	1.12	1.92	0.21	0.74	0.95	118	202	0.2
	2–5	460	0.26	0.82	1.83	0.15	0.62	0.77	106	238	0.15
6014	0–2	492	0.32	0.31	0.07	0.06	0.02	0.08	388	88	0.07
6015	0–2	468	0.43	0.47	0.25	0.09	0.05	0.14	336	179	0.04
6016	0–2	459	0.39	1.52	3.38	0.37	1.01	1.38	110	245	0.2
	2–5	457	0.37	1.2	2.26	0.22	0.97	1.19	101	190	0.23
6027	0–2	386	0.17	1.01	1.98	0.17	0.47	0.64	158	309	0.2
	2–5	375	0.31	1.12	1.27	0.17	0.43	0.6	187	212	0.13
6045	0–2	380	0.33	1.22	1.86	0.2	0.59	0.79	154	235	0.2
	2–5	372	0.27	0.49	2.03	0.13	0.56	0.69	71	294	0.5
6053	0–2	390	0.34	1.52	3.32	0.28	0.98	1.26	121	263	0.2
	2–5	384	0.48	1.5	2.26	0.26	0.95	1.21	124	187	0.18

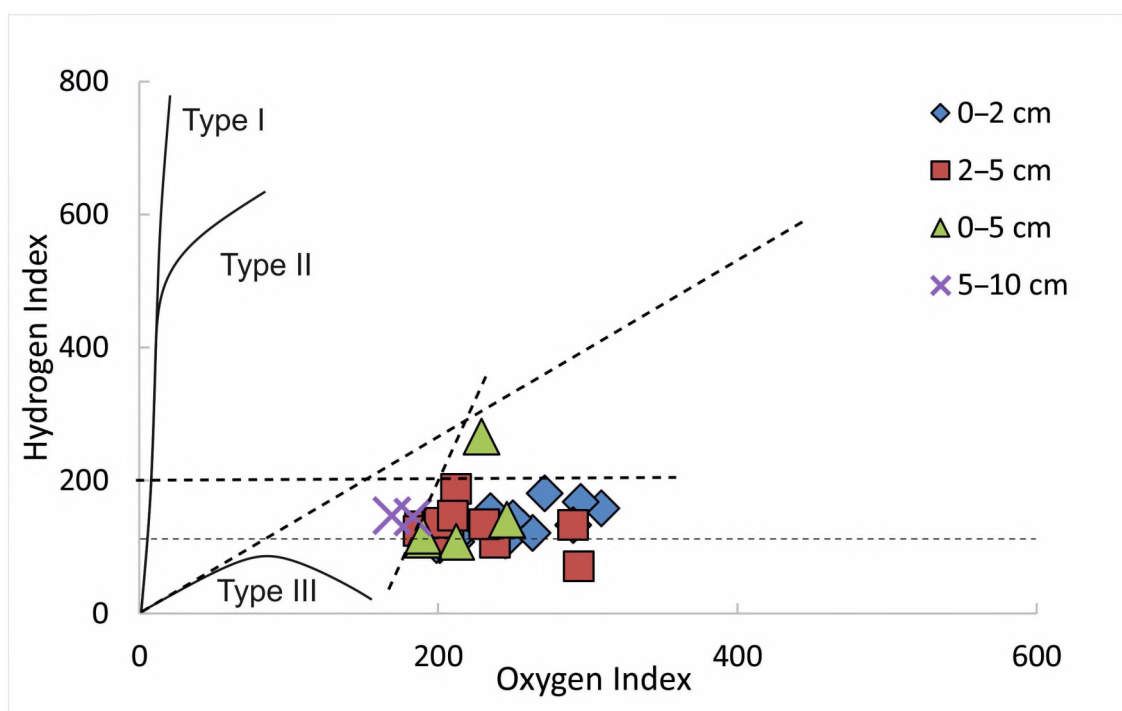


Table 2. Cont.

Station	Sampling Horizon	T <sub>peak</sub> , °C <sup>a</sup>	S1 <sup>b</sup> , mgHC/TOC	S2 <sup>b</sup> , mgHC/TOC	S3 <sup>b</sup> , mgCO <sub>2</sub> /TOC	PC <sup>c</sup> , %	RC <sup>c</sup> , %	TOC <sup>c</sup> , %	HI <sup>d</sup>	OI <sup>d</sup>	MinC <sup>c</sup> , %
6056	0–2	380	0.19	1	1.75	0.16	0.54	0.7	143	250	0.2
	2–5	372	0.16	0.86	1.48	0.14	0.5	0.64	134	231	0.14
6058	0–2	369	0.11	0.87	1.3	0.13	0.35	0.48	181	271	0.1
	2–5	383	0.26	1.01	1.49	0.16	0.58	0.74	136	201	0.14
6065	0–2	380	0.11	0.67	1.18	0.11	0.29	0.4	168	295	0.1
	2–5	374	0.16	0.75	1.07	0.12	0.39	0.51	147	210	0.12
6068	0–2	401	0.19	0.92	2	0.16	0.53	0.69	133	290	0.2
	2–5	401	0.19	0.92	2	0.16	0.53	0.69	133	290	0.15
6490	0–5	462	0.63	2.92	5.74	0.5	2.21	2.71	108	212	0.38
	5–10	458	1.36	3.49	4.38	0.57	1.83	2.4	145	183	0.31
6491	0–5	462	0.75	2.8	4.79	0.47	2.05	2.52	111	190	0.29
6505	0–5	396	0.61	1.49	2.41	0.36	0.91	1.27	117	190	0.2
	5–10	387	0.8	1.57	1.81	0.26	0.81	1.07	147	169	0.19
6521	0–5	374	1.01	1.81	1.56	0.28	0.4	0.68	266	229	0.11
6527	0–5	379	0.46	1.42	2.48	0.25	0.76	1.01	141	246	0.17

<sup>a</sup> T<sub>peak</sub>—the temperature of peak S2 yield. <sup>b</sup> S1—S1 carbon peak including free hydrocarbons and low molecular weight OM, mg HC/g; S2—S2 carbon peak including hydrogen rich OM, mg HC/g; S3—S3 carbon peak including oxygen-containing OM, mg CO<sub>2</sub>/g. <sup>c</sup> PC—pyrolyzable carbon; RC—residual carbon; MinC—mineral carbon; TOC—Total organic carbon All units are calculated in wt%. <sup>d</sup> HI—Hydrogen Index; OI—Oxygen Index. RE parameters for the horizon 0–2 cm have been reported earlier in [53]. Samples 6014 and 6015 are not included in the reported RE statistics because of their potential erroneous calculations (due to extremely low TOC values).

HI values generally were within the range of 100–200 mg HC/g TOC with only one sample exceeding 250 mg HC/g TOC. We excluded samples 6014 and 6015 with extremely low TOC values, which might result in incorrect RE determination. OI values fell between 200 and 300 CO<sub>2</sub>/g TOC (Figure 2). As mentioned earlier, OI corresponds to the S3 peak (quantity of CO<sub>2</sub> relative to TOC), which is likely to increase during degradation/oxidation processes [31,52]. The relationship between HI and OI presented as a Van Krevelen-type diagram has been widely used to distinguish between organic matter sources. HI and OI plotted on this diagram showed that almost all values fell within the limited area indicating that the modern OM stored in the surface sediments had relatively low proportion of hydrocarbons and a higher content of oxygen-containing compounds. This points to the similar OM nature for the modern sediments as for Type II (planktonic) and Type III (humic) kerogen in ancient sediments.



**Figure 2.** Van Krevelen-type diagram of surface sediments in LS. Each symbol represents one horizon of the sediment core indicated in the legend. Curved lines I, II and III represent kerogen types for the ancient sediments and matured OM (algal/sapropelic, planktonic and humic, respectively). Dashed line represents HI = 100. Bold dashed line represents HI/OI = 1. Blue rhombs, red squares, green triangles and lilac crosses represent different sediment sampling horizons: 0–2 cm, 2–5 cm, 0–5 cm and 5–10 cm, respectively.

The generally low HI and HI/OI values across the LS sediments suggest a high degree of OM degradation and/or significant contribution from terrestrial OM sources [28,31]. For the outer shelf sediments, the HI/OI ratios were slightly higher (but still not exceeding 1.1). These results indicate a generally highly degraded sedimentary OM with growing contribution of fresher and/or more marine OM with increasing distance from the coastline. Overall, our data agree with previous findings for the LS surface sediments reported in [36] where HI/OI values fell within a range of 0.5–1. Similar values were also observed for the sediment cores of the Hudson bay [28].

Neither HI nor OI correlated with the sampling depth (Supplementary Materials Figure S1), we divided the samples into two groups based on the distance from the coastline. Inner and mid-shelf sediments (stations 6005–6016, 6490–6491 and 6505) had relatively low HI (<130 mg HC/g TOC, average 115 mg HC/g) and OI (<245 CO<sub>2</sub>/g TOC, average 202 CO<sub>2</sub>/g TOC). Meanwhile, the majority of the outer shelf sediments (stations 6027–6527) was characterized by elevated HI and OI ratios (average

150 mg HC/g TOC and 243 CO<sub>2</sub>/g TOC, respectively; Figure 3a–d). Previous studies of the Arctic and subarctic shelf seas sediments reported HI values higher than 100 mg HC/g TOC to be found almost exclusively in the offshore areas. Thus, a threshold of 100 mg HC/g TOC has been proposed as a shift from terrigenous to marine OM sources [28,36,70]. Slightly higher HI distinction (130 mg HC/g TOC) between primary marine and terrestrial sources observed for the studied sediments may be attributed to the portion of remobilized old terrestrial OM produced during the short vegetative seasons and preserved with little degradation in the “deep freezer” of the Eastern Arctic [4,71]. Previous studies showed that high HI values detected in Early Holocene and Late Pleistocene (Yedoma) permafrost deposits might correspond to a higher aliphatic character of the OM and therefore to indicate a better quality of OM in respect to active microbial degradation [39].

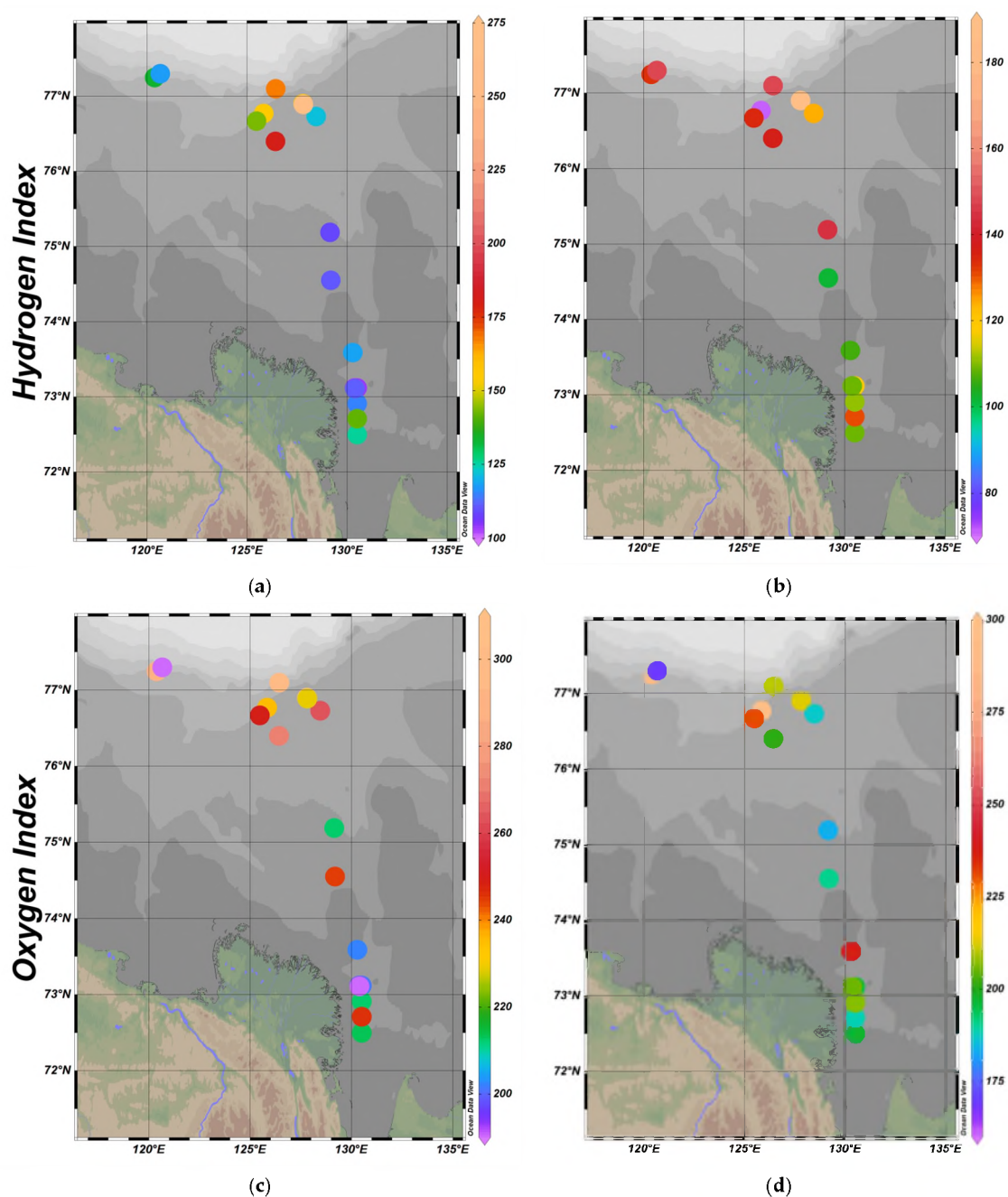
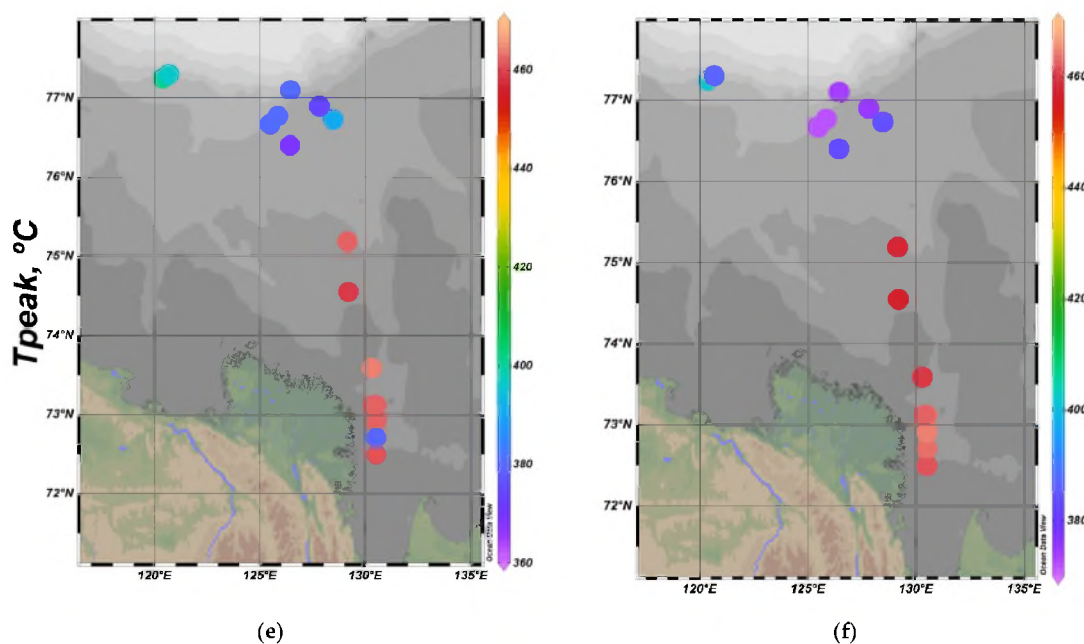
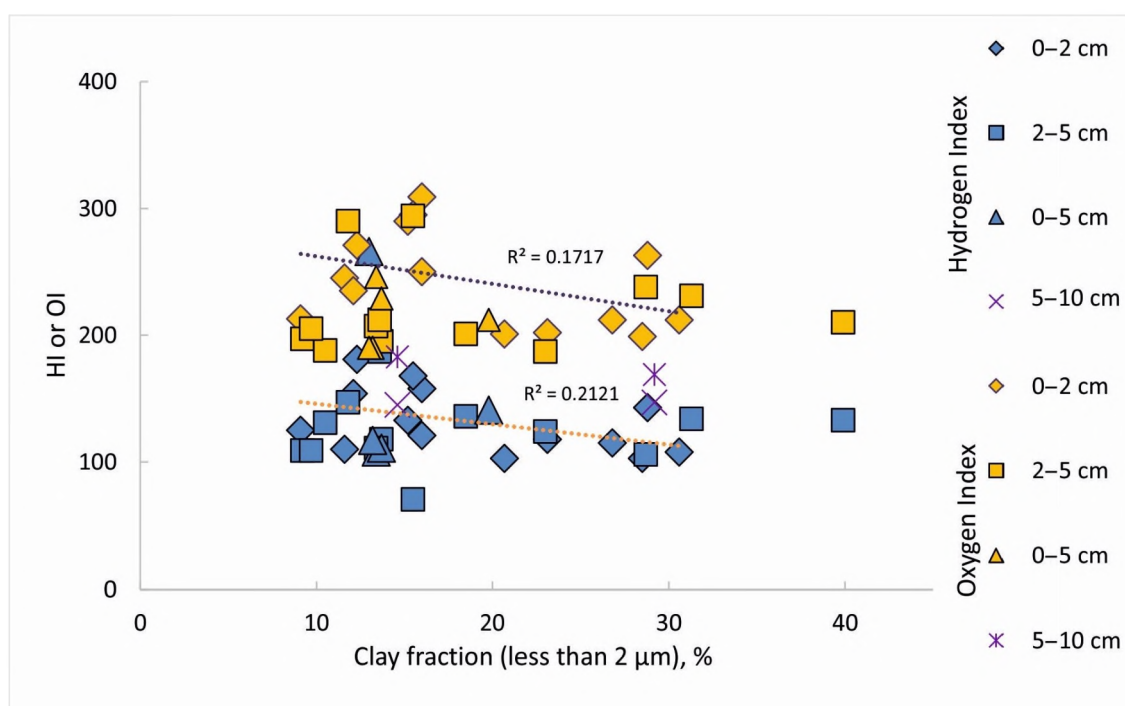


Figure 3. Cont.



**Figure 3.** Distribution of Rock-Eval parameters for LS surface sediments: HI (a,b); OI (c,d) and  $T_{peak}$  °C (e,f). Figure 3a,c,e show values for the uppermost sampling horizon 0–2 cm (for stations 6490, 6491, 6505, 6521 and 6527—0–5 cm); Figure 3b,d,f show values for the underlying sampling horizon 2–5 cm (for stations 6490 and 6505—5–10 cm).

No obvious correlations were observed for the HI and OI values and particle size of the sediments. We showed a weak positive correlation between HI, OI and the fraction of clay-sized particles (less than 2  $\mu\text{m}$  in diameter) for only the uppermost sediment layer (0–2 cm), which also could not be interpreted as a strong linear relationship (Figure 4). Thus, in contrast with previous findings, our results did not provide any evidence on neither special protection of the mineral-bound OM [28,72–74] nor OM exposition to oxidation during repeated resuspension of the fine particles [28].



**Figure 4.** The relationship between HI and OI and the clay-sized fraction in LS surface sediments.

$T_{\text{peak}}$  values varied from 369 to 464 °C across all sediments but were predominantly clustered in two major groups ranging from 369 to 401 °C and from 451 to 464 °C, neither of which was linearly related to HI or OI (Figure S2). The low  $T_{\text{peak}}$  group demonstrated a rather homogenous distribution of the full range of OI values and slightly higher HI ratios compared to the high  $T_{\text{peak}}$  group. Generally  $T_{\text{peak}}$  measurements represent the thermal stability of OM compounds indicating its potential source. The high  $T_{\text{peak}}$  results are typical for decomposition of immature humic substances (420–470 °C), which were detected for organo-mineral soil horizons by [75]. Nevertheless, some regional contrasts for the ESAS permafrost carbon pools should be addressed. In particular, the extensive East Siberian Arctic coastline is dominated by Pleistocene ice complex deposits. As estimated by [3], carbon remobilized from the ice complex deposit constitutes 36–76% of the sedimentary organic carbon across the shelf, despite its mostly coastal supply, while carbon released from the topsoil permafrost contributes only from 35% to 5% with increasing distance from the land. It has been shown that, in contrast to most thawed mineral soils, relict soils of the ice complex generally contain little of the humus and have high carbon concentration [76]. Nevertheless, we still observe high  $T_{\text{peak}}$  values across the shallow and mid shelf areas (Figure 3e,f). These values together with elevated HI terrestrial vs. marine threshold (130 mg HC/g TOC) point to contribution of different permafrost-carbon sources arising from both the seasonally thawing active layer and Pleistocene ice rich deposits. This is in good agreement with findings of [3] on the permafrost-derived carbon distribution across the shelf sediments.

The shift from high  $T_{\text{peak}}$  values near the coastlines to low  $T_{\text{peak}}$  range on the outer shelf reflects an increasing contribution of labile autochthonous compounds and shorter hydrocarbon chains. Low temperatures are typical for more recent organic matter reflecting the thermal breakdown of biological constituents such as polysaccharides and lignin and/or cellulose [75] or high deoxy sugar content associated with active microbial degradation in fine particulate OM as proposed by [31,77]. The abundances of lignin phenol proxies across the East Siberian Arctic shelf have been widely investigated by previous researchers [11–13,78,79]. As reported in [11], lignin concentrations along the Laptev Sea transect decreased by more than 2 orders of magnitude with increasing distance from the coast. Thus, the low  $T_{\text{peak}}$  results hardly represent lignin compounds but most likely reflect a higher concentration of deoxy sugars derived from bacteria or plankton [80,81]. This hypothesis is supported by overall high clay and fine silt content across the outer shelf except the “coarse-grained” zones mentioned earlier. Moreover, the low  $T_{\text{peak}}$  values together with the elevated OI ratios detected on the outer shelf may indicate a significant contribution of short-chained hydrocarbons, which become oxygenated during microbial activity [28,82].

### 3.3. Sedimentary OM Composition on the Molecular Level

High molecular weight (HMW;  $\geq C_{21}$ ) n-alkanes and n-alkanoic acids are derived from terrestrial higher plant waxes [83] producing a molecular signal of terrestrial contribution while low molecular weight (LMW;  $\leq C_{19}$ ) lipids were used as tracers of algal-derived OM.

Concentrations of both HMW n-alkanes and HMW n-alkanoic acids in surface sediments decreased significantly from the shallow depths to the outer shelf ranging from 4.1 to 0.1 mg g<sup>-1</sup> OC for the HMW n-alkanes and from 4.6 to 0.1 mg g<sup>-1</sup> OC for the HMW n-acids (Table 3). The results were similar to the concentrations reported in [11,13,84] for the same study area. A strong terrestrial signal of HMW to LMW n-alkanes ratio was traced along the studied transect within a range of 2.7–77.7, which corroborates with previous results reported for the Buor-Khaya Bay [6,13]. These findings revealed a dominating input of the terrestrial source to sedimentary OM not only near the Lena River mouth but also off to the deeper basins.

**Table 3.** Molecular markers of the LS surface sediments.

Station	Sampling Horizon	HMW n-Alkanes <sup>a</sup> , µg/g dw sed	HMW n-Alkanes <sup>a</sup> , mg/g OC	HMW/LMW <sup>b</sup> n-Alk	HMW n-Alk CPI <sup>c</sup>	TAR <sup>d</sup>	OEP <sub>26-33</sub> <sup>e</sup>	HMW n-Alk Acids <sup>a</sup> , µg/g dw sed	HMW n-Alk Acids <sup>a</sup> , mg/g OC	HMW n-Alk Acids/n-Alk <sup>a</sup>
6005	0–2	6.18	0.44	23.79	3.92	21.00	3.93	29.82	2.10	4.83
	2–5	8.56	0.62	10.19	6.50	4.02	6.23	18.53	1.33	2.16
6006	0–2	18.42	0.68	37.83	6.87	45.70	6.95	14.16	0.52	0.77
	2–5	2.65	0.10	10.06	6.91	4.77	6.87	11.45	0.45	4.33
6007	0–2	11.44	1.00	49.68	5.75	28.75	5.81	21.07	0.80	1.84
	2–5	23.76	0.97	13.43	7.83	5.77	7.68	30.37	1.24	1.28
6008	0–2	31.95	1.41	77.71	10.00	65.24	10.24	38.13	1.68	1.19
	2–5	27.06	1.25	6.93	7.78	4.24	7.37	38.80	1.80	1.43
6009	0–2	57.09	2.96	53.54	7.59	45.86	7.77	60.29	3.12	1.06
	2–5	40.29	2.13	12.75	9.84	5.74	9.57	15.28	0.81	0.38
6013	0–2	6.15	0.65	42.26	5.97	41.31	5.87	5.54	0.58	0.90
	2–5	31.89	4.14	4.64	5.59	1.81	5.35	20.28	2.63	0.64
6016	0–2	4.59	0.33	25.47	1.56	8.81	1.12	11.91	0.86	2.59
	2–5	18.16	1.53	3.54	4.71	1.34	4.32	48.91	4.11	2.69
6027	0–2	2.36	0.37	14.34	3.60	10.65	3.59	2.70	0.42	1.14
	2–5	6.72	1.12	2.68	3.26	0.94	3.04	10.61	1.77	1.58
6045	0–2	2.16	0.27	22.99	2.57	12.30	2.73	4.19	0.53	1.94
	2–5	6.93	1.00	4.67	3.80	2.04	3.57	7.77	1.13	1.12
6053	0–2	2.18	0.17	21.95	3.60	15.02	3.37	2.16	0.17	0.99
	2–5	17.39	1.44	24.05	4.69	13.06	4.31	14.31	1.18	0.82
6056	0–2	2.22	0.32	25.45	4.16	17.02	4.10	1.93	0.28	0.87
	2–5	2.97	0.46	11.99	3.00	6.21	2.70	2.39	0.37	0.81
6058	0–2	1.00	0.21	4.17	2.03	1.92	2.11	0.90	0.19	0.90
	2–5	2.64	0.36	4.91	4.16	2.51	3.73	2.46	0.33	0.93
6065	0–2	1.16	0.29	7.69	2.31	5.69	3.17	0.31	0.08	0.27
	2–5	3.92	0.77	3.15	4.23	1.36	4.15	2.92	0.57	0.75
6068	0–2	2.58	0.37	3.50	2.18	2.42	2.02	5.23	0.76	2.03
	2–5	1.04	0.15	5.63	6.65	3.75	6.88	6.13	0.89	5.88
6490	0–5	4.91	0.18	46.86	4.57	21.80	4.32	9.48	0.40	1.93
	5–10	13.18	0.55	58.15	8.36	45.14	8.40	21.26	0.78	1.61
6505	0–5	1.72	0.14	21.34	3.02	11.06	2.71	3.13	0.25	1.83
	5–10	1.70	0.16	52.14	5.82	36.28	5.76	1.72	0.16	1.01
6527	0–5	1.18	0.12	16.27	5.13	9.30	4.93	1.34	0.13	1.13

<sup>a</sup> T<sub>peak</sub>—the temperature of peak S2 yield. <sup>b</sup> S1—S1 carbon peak including free hydrocarbons and low molecular weight OM, mg HC/g; S2—S2 carbon peak including hydrogen rich OM, mg HC/g; S3—S3 carbon peak including oxygen-containing OM, mg CO<sub>2</sub>/g. <sup>c</sup> PC—pyrolyzable carbon; RC—residual carbon; MinC—mineral carbon; TOC—Total organic carbon All units are calculated in wt%. <sup>d</sup> HI—Hydrogen Index; OI—Oxygen Index. <sup>e</sup> Parameters for the horizon 0–2 cm have been reported earlier in [53].

We calculated a suite of widely used molecular ratios in order to provide an additional insight into the relative contribution of terrestrial OM sources in marine sediments and its degradation state [6,13,36,85]. High values ( $>5$ ) of the carbon preference index (CPI) are typically attributed to fresh and more labile OM, and this ratio decreases toward 1 during ongoing degradation [86,87]. For the studied sediments, CPI values vary from 10 to 1.56 decreasing off to the continental slope (Figure 5a), which is comparable with previous CPI values reported for ESAS sediments [6,13]. A significant increase of CPI is observed for deeper sampling horizons (0–2 cm vs. 2–5 cm; 0–5 cm vs. 5–10 cm for the stations 6490 and 6505) indicating less degraded material stored in deeper layers (Figure 5b). Moreover, HMW n-alkane CPI ratios are correlated with S2 parameter indicating a proportion of hydrogen-rich OM and aliphatic OM character, more susceptible to degradation and preferable for greenhouse gas generating microorganisms (Figure S3) [39,88]. Odd-over-even predominance (OEP) usually decreasing with degradation showed the same values range (from 10.24 to 1.12) and, similar to CPI, considerably increasing with sediment sampling depth. Terrigenous-to-aquatic ratio (TAR) ranged from 1 to 65 decreasing both off to the outer shelf and to the deeper layers. For most 2–5 cm sampling horizons, TAR drastically declined by an order of magnitude if compared to the uppermost layer.

Decreasing HMW n-alkanoic acid/n-alkane ratio (Table 1) reflected the loss of the carboxyl group with ongoing degradation, which made it a well-used indicator of terrestrial OM degradation state. HMW n-alkanoic acid/n-alkane ratios varied between 0.27 and 6.99 (Figure 5c) similarly to those reported in [13] for the Buor-Khaya Bay located near the Lena delta. Similar to other molecular proxies the acid/alkane ratio span a large range of degradation states indicating both a significant contribution of recent OM in shallow and mid shelf areas and much more degraded terrestrial matter on the outer shelf. Nevertheless, we did not observe any expected correlations between the sampling layers (Figure 5d). This may be attributed to the different local contributions of degraded OM over the last decades across the continental margin. Similarly, Bröder et al. [11] reported an increasing trend of HMW acids/alkanes ratio with increasing depth (down to 30–40 cm) throughout the sediment core taken from the East Siberian Sea coastal zone and an opposite trend for the core from the outer shelf.

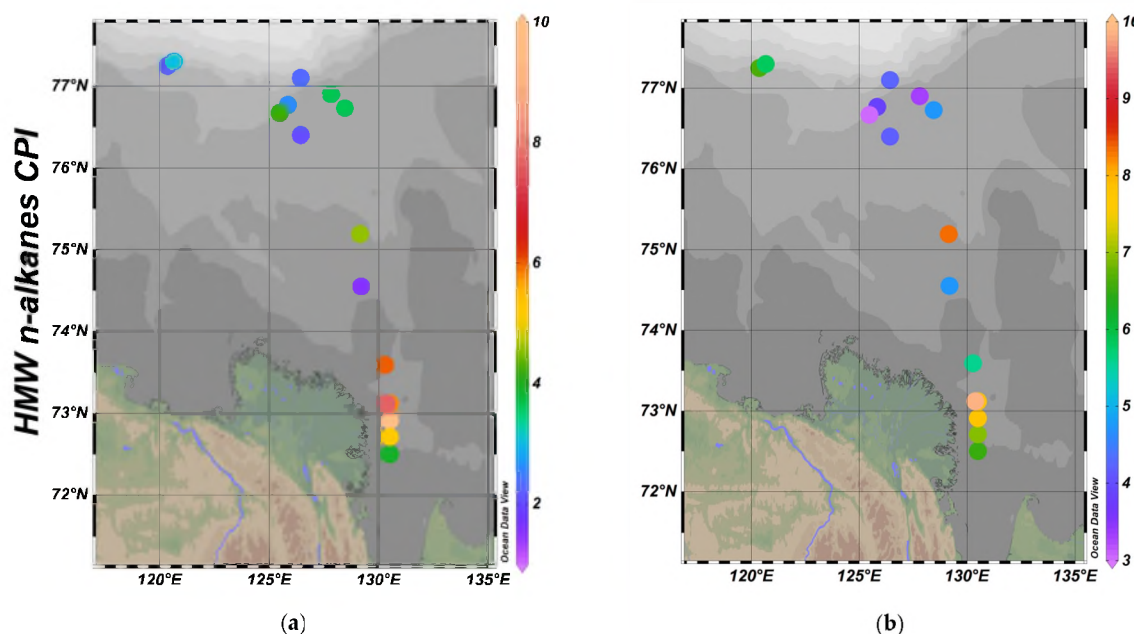
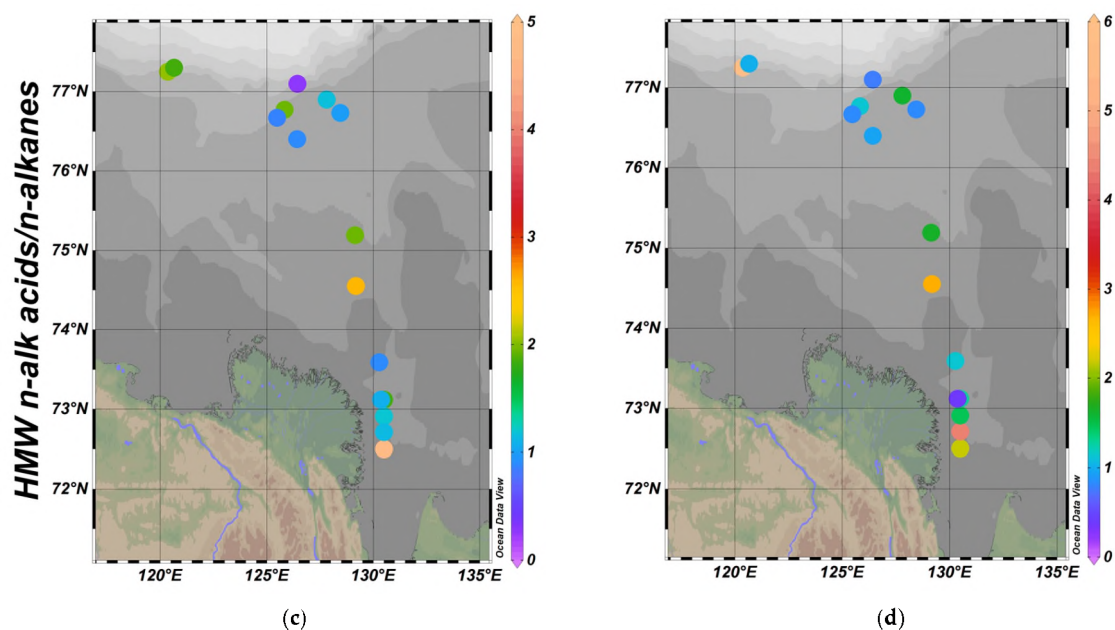


Figure 5. Cont.



**Figure 5.** Distribution of molecular ratios for LS surface sediments: high molecular weight (HMW) n-alkanes carbon preference index (CPI; **a,b**); HMW n-alkanoic acids/HMW n-alkanes (**c,d**). Figure 5a,c show values for the uppermost sampling horizon 0–2 cm (for stations 6490, 6491, 6505, 6521 and 6527–0–5 cm); Figure 5b,d show values for the underlying sampling horizon 2–5 cm (for stations 6490 and 6505—5–10 cm).

#### 4. Conclusions

A combined geochemical investigation of recent sedimentary OM stored in the LS surface sediments was performed using both the RE pyrolysis data and traditional molecular proxies along with bulk grain-size characteristics. We observed the overall accumulation of the fine-grained (<63  $\mu\text{m}$ ) surface sediments controlled by stable subglacial sedimentation environment. Coarse-grained sediments areas detected on the mid and outer shelf might be a result of several external hydrodynamic factors including exaration processes, gas venting or brine injections. Meanwhile, highly degraded sedimentary OM seemed to be dominating OM fraction across the entire studied profile with some growing portion of fresher and/or more marine OM on the outer shelf, which was confirmed by HI/OI values and molecular ratios. In contrast to previous RE reports, a slightly elevated HI of 130 mg HC/g TOC was proposed as a threshold indicating a shift from terrigenous to marine OM sources for the LS shelf. A clear distinction between highly degraded and fresher OM was observed for the  $T_{\text{peak}}$  values ranging within two major groups from 369 to 401  $^{\circ}\text{C}$  and from 451 to 464  $^{\circ}\text{C}$  for the outer shelf and for the shallow and mid shelf, respectively. These values together are supposed to represent terrestrial permafrost-carbon pools exporting from both the seasonally thawing active layer and Pleistocene ice rich deposits. These results corroborate with the interpretation of molecular markers (n-alkanes and n-alkanoic acids), which trace an intensive degradation along the coastline-outer shelf profile. However, a contrasting trend is observed for the different sampling horizon indicating a much less degraded material stored in deeper layers. This confirms the notion reported by previous researchers that the most active degradation takes part during the cross-shelf transport, not while getting buried deeper.

Generally, RE may provide a useful characterization of the OM distribution, sources and degradation state across the LS that may be successfully applied along with traditional geochemical tracers in order to contribute to understanding of the Arctic biogeochemical regimes.

**Supplementary Materials:** The following are available online at <http://www.mdpi.com/2073-4441/12/12/3511/s1>, Figure S1: Hydrogen Index (a) and Oxygen Index (b) vs. Water depth, m for LS surface sediments, Figure S2: Hydrogen Index (a) and Oxygen Index (b) vs.  $T_{\text{peak}}$ ,  $^{\circ}\text{C}$  for LS surface sediments, Figure S3: S<sub>2</sub>, mgHC/TOC vs. HMW n-alkanes CPI for LS surface sediments.



**Author Contributions:** E.G., I.O., E.K., N.P. A.L. and A.G. contributed to the sample preparation and measurements, E.G., N.G. and I.S. were involved in planning and supervised the work, E.G. processed the experimental data, performed the analysis, drafted the manuscript and designed the figures. A.R., E.K., N.P., A.G., D.C. performed the fieldwork. All authors discussed the results and commented on the manuscript. All authors have read and agreed to the published version of the manuscript.

**Funding:** This research was supported by the Russian Science Foundation (laboratory analyses and interpretation were performed within the project No. 19-77-00067) and Tomsk Polytechnic University Competitiveness Enhancement Program (expeditions and sampling).

**Acknowledgments:** Authors are thankful to Ivan V. Goncharov for his invaluable contribution into the Arctic carbon studies at Tomsk polytechnic university. Authors thank three anonymous reviewers for their constructive comments, which led to significant improvement of the manuscript.

**Conflicts of Interest:** The authors declare no conflict of interest.

## References

- Hugelius, G.; Strauss, J.; Zubrzycki, S.; Harden, J.W.; Schuur, E.A.G.; Ping, C.L.; Schirmer, L.; Grosse, G.; Michaelson, G.J.; Koven, C.D.; et al. Estimated stocks of circumpolar permafrost carbon with quantified uncertainty ranges and identified data gaps. *Biogeosciences* **2014**, *11*, 6573–6593. [[CrossRef](#)]
- Shakhova, N.; Semiletov, I.; Leifer, I.; Salyuk, A.; Rekan, P.; Kosmach, D. Geochemical and geophysical evidence of methane release over the East Siberian Arctic Shelf. *J. Geophys. Res. Ocean.* **2010**, *115*. [[CrossRef](#)]
- Vonk, J.E.; Sanchez-Garcia, L.; Van Dongen, B.E.; Alling, V.; Kosmach, D.; Charkin, A.; Semiletov, I.P.; Dudarev, O.V.; Shakhova, N.; Roos, P.; et al. Activation of old carbon by erosion of coastal and subsea permafrost in Arctic Siberia. *Nature* **2012**. [[CrossRef](#)] [[PubMed](#)]
- Vonk, J.E.; Sánchez-García, L.; Semiletov, I.; Dudarev, O.; Eglinton, T.; Andersson, A.; Gustafsson, O. Molecular and radiocarbon constraints on sources and degradation of terrestrial organic carbon along the Kolyma paleoriver transect, East Siberian Sea. *Biogeosciences* **2010**, *7*, 3153–3166. [[CrossRef](#)]
- Vonk, J.E.; Gustafsson, Ö. Permafrost-carbon complexities. *Nat. Geosci.* **2013**, *6*, 675–676. [[CrossRef](#)]
- Van Dongen, B.E.; Semiletov, I.; Weijers, J.W.H.; Gustafsson, Ö. Contrasting lipid biomarker composition of terrestrial organic matter exported from across the Eurasian Arctic by the five great Russian Arctic rivers. *Glob. Biogeochem. Cycles* **2008**, *22*. [[CrossRef](#)]
- Semiletov, I.P. Aquatic sources and sinks of CO<sub>2</sub> and CH<sub>4</sub> in the polar regions. *J. Atmos. Sci.* **1999**, *56*, 286–306. [[CrossRef](#)]
- Semiletov, I. The failure of coastal frozen rock as an important factor in the biogeochemistry of the Arctic shelf water. *Dokl. Earth Sci.* **1999**, *369*, 1140–1143.
- Semiletov, I.P.; Shakhova, N.E.; Pipko, I.I.; Pugach, S.P.; Charkin, A.N.; Dudarev, O.V.; Kosmach, D.A.; Nishino, S. Space-time dynamics of carbon and environmental parameters related to carbon dioxide emissions in the Buor-Khaya Bay and adjacent part of the Laptev Sea. *Biogeosciences* **2013**, *10*, 5977–5996. [[CrossRef](#)]
- Semiletov, I.; Pipko, I.; Gustafsson, Ö.; Anderson, L.G.; Sergienko, V.; Pugach, S.; Dudarev, O.; Charkin, A.; Gukov, A.; Bröder, L.; et al. Acidification of East Siberian Arctic Shelf waters through addition of freshwater and terrestrial carbon. *Nat. Geosci.* **2016**, *9*, 361–365. [[CrossRef](#)]
- Bröder, L.; Tesi, T.; Salvadó, J.A.; Semiletov, I.P.; Dudarev, O.V.; Gustafsson, Ö. Fate of terrigenous organic matter across the Laptev Sea from the mouth of the Lena River to the deep sea of the Arctic interior. *Biogeosciences* **2016**, *13*, 5003–5019. [[CrossRef](#)]
- Tesi, T.; Semiletov, I.; Hugelius, G.; Dudarev, O.; Kuhry, P.; Gustafsson, Ö. Composition and fate of terrigenous organic matter along the Arctic land-ocean continuum in East Siberia: Insights from biomarkers and carbon isotopes. *Geochim. Cosmochim. Acta* **2014**. [[CrossRef](#)]
- Karlsson, E.S.; Charkin, A.; Dudarev, O.; Semiletov, I.; Vonk, J.E.; Sánchez-García, L.; Andersson, A. Carbon isotopes and lipid biomarker investigation of sources, transport and degradation of terrestrial organic matter in the Buor-Khaya Bay, SE Laptev Sea. *Biogeosciences* **2011**, *8*, 1865–1879. [[CrossRef](#)]
- Karlsson, E.S.; Brüchert, V.; Tesi, T.; Charkin, A.; Dudarev, O.; Semiletov, I.; Gustafsson, O. Contrasting regimes for organic matter degradation in the East Siberian Sea and the Laptev Sea assessed through microbial incubations and molecular markers. *Mar. Chem.* **2015**. [[CrossRef](#)]
- Semiletov, I.P.; Shakhova, N.E.; Sergienko, V.I.; Pipko, I.I.; Dudarev, O.V. On carbon transport and fate in the East Siberian Arctic land-shelf-atmosphere system. *Environ. Res. Lett.* **2012**, *7*, 015201. [[CrossRef](#)]

16. Doğrul Selver, A.; Sparkes, R.B.; Bischoff, J.; Talbot, H.M.; Gustafsson, Ö.; Semiletov, I.P.; Dudarev, O.V.; Boulton, S.; van Dongen, B.E. Distributions of bacterial and archaeal membrane lipids in surface sediments reflect differences in input and loss of terrestrial organic carbon along a cross-shelf Arctic transect. *Org. Geochem.* **2015**. [[CrossRef](#)]
17. Sparkes, R.B.; Selver, A.D.; Gustafsson, Ö.; Semiletov, I.P.; Haghipour, N.; Wacker, L.; Eglinton, T.I.; Talbot, H.M.; Van Dongen, B.E. Macromolecular composition of terrestrial and marine organic matter in sediments across the East Siberian Arctic Shelf. *Cryosphere* **2016**. [[CrossRef](#)]
18. Charkin, A.N.; Dudarev, O.V.; Semiletov, I.P.; Kruhmalev, A.V.; Vonk, J.E.; Sánchez-García, L.; Karlsson, E.; Gustafsson, O. Seasonal and interannual variability of sedimentation and organic matter distribution in the Buor-Khaya Gulf: The primary recipient of input from Lena River and coastal erosion in the southeast Laptev Sea. *Biogeosciences* **2011**. [[CrossRef](#)]
19. Tesi, T.; Semiletov, I.; Dudarev, O.; Andersson, A.; Gustafsson, Ö. Matrix association effects on hydrodynamic sorting and degradation of terrestrial organic matter during cross-shelf transport in the Laptev and East Siberian shelf seas. *J. Geophys. Res. Biogeosci.* **2016**. [[CrossRef](#)]
20. Dudarev, O.V.; Semiletov, I.P.; Charkin, A.N.; Botsul, A.I. Deposition settings on the continental shelf of the east Siberian sea. *Dokl. Earth Sci.* **2006**, *409*, 1000–1005. [[CrossRef](#)]
21. Lafargue, E.; Marquis, F.; Pillot, D. Rock-Eval 6 applications in hydrocarbon exploration, production, and soil contamination studies. *Rev. l'Institut Fr. Pet.* **1998**, *53*, 421–437. [[CrossRef](#)]
22. Köster, J.; Kotarba, M.; Lafargue, E.; Kosakowski, P. Source rock habitat and hydrocarbon potential of Oligocene Menilite Formation (Flysch Carpathians, Southeast Poland): An organic geochemical and isotope approach. *Org. Geochem.* **1998**, *29*, 543–558. [[CrossRef](#)]
23. Demirel, I.H.; Kozlu, H. Evaluation of burial history, thermal maturity and source-rock assessment of the Upper Paleozoic succession of the eastern Taurus region, southern Turkey. *Mar. Pet. Geol.* **1997**, *14*, 867–877. [[CrossRef](#)]
24. Behar, F.; Beaumont, V.; De, H.L. Technologie Rock-Eval 6: Performances et développements. *Oil Gas Sci. Technol.* **2001**, *56*, 111–134. [[CrossRef](#)]
25. Peskova, D.N.; Sizykh, A.V.; Rukavishnikov, V.S. Evaluation the value-of-information (VOI) and look back analysis during modelling of the exploration works. In Proceedings of the 7th EAGE Saint Petersburg International Conference and Exhibition: Understanding the Harmony of the Earth's Resources Through Integration of Geosciences, Saint Petersburg, Russia, 11–14 April 2016; pp. 494–498.
26. Kharitontseva, P.A.; Rukavishnikov, V.S.; Geiger, S. DFN modelling and upscaling of the naturally fractured field. In Proceedings of the Geomodel 2017—19th Science and Applied Research Conference on Oil and Gas Geological Exploration and Development; European Association of Geoscientists and Engineers, Gelendzhik, Russia, 11–14 September 2017; Volume 2017, pp. 1–5.
27. Sebag, D.; Disnar, J.R.; Guillet, B.; Di Giovanni, C.; Verrecchia, E.P.; Durand, A. Monitoring organic matter dynamics in soil profiles by “Rock-Eval pyrolysis”: Bulk characterization and quantification of degradation. *Eur. J. Soil Sci.* **2006**, *57*, 344–355. [[CrossRef](#)]
28. Hare, A.A.; Kuzyk, Z.Z.A.; Macdonald, R.W.; Sanei, H.; Barber, D.; Stern, G.A.; Wang, F. Characterization of sedimentary organic matter in recent marine sediments from Hudson Bay, Canada, by Rock-Eval pyrolysis. *Org. Geochem.* **2014**, *68*, 52–60. [[CrossRef](#)]
29. Disnar, J.R.; Trichet, J. The influence of various divalent cations (UO<sub>2</sub><sup>2+</sup>, Cu<sup>2+</sup>, Pb<sup>2+</sup>, Co<sup>2+</sup>, Ni<sup>2+</sup>, Zn<sup>2+</sup>, Mn<sup>2+</sup>) on the thermally induced evolution of organic matter isolated from an algal mat. *Org. Geochem.* **1984**, *6*, 865–874. [[CrossRef](#)]
30. Baudin, F.; Stetten, E.; Schnyder, J.; Charlier, K.; Martinez, P.; Dennielou, B.; Droz, L. Origin and distribution of the organic matter in the distal lobe of the Congo deep-sea fan—A Rock-Eval survey. *Deep. Res. Part II Top. Stud. Oceanogr.* **2017**, *142*, 75–90. [[CrossRef](#)]
31. Marchand, C.; Lallier-Vergès, E.; Disnar, J.R.; Kérais, D. Organic carbon sources and transformations in mangrove sediments: A Rock-Eval pyrolysis approach. *Org. Geochem.* **2008**, *39*, 408–421. [[CrossRef](#)]
32. Leonova, G.A.; Mal'tsev, A.E.; Melenevskii, V.N.; Miroshnichenko, L.V.; Kondrat'eva, L.M.; Bobrov, V.A. Geochemistry of Diagenesis of Organogenic Sediments: An Example of Small Lakes in Southern West Siberia and Western Baikal Area. *Geochem. Int.* **2018**, *56*, 344–361. [[CrossRef](#)]

33. Melenevskii, V.N.; Leonova, G.A.; Bobrov, V.A.; Kashirtsev, V.A.; Krivonogov, S.K. Transformation of organic matter in the Holocene sediments of Lake Ochki (south Baikal region): Evidence from pyrolysis data. *Geochem. Int.* **2015**, *53*, 903–921. [[CrossRef](#)]
34. Melenevskii, V.N.; Leonova, G.A.; Konyshov, A.S. The organic matter of the recent sediments of Lake Beloe, West Siberia (from data of pyrolytic studies). *Russ. Geol. Geophys.* **2011**, *52*, 583–592. [[CrossRef](#)]
35. Fahl, K.; Stein, R. Biomarker records, organic carbon accumulation, and river discharge in the Holocene southern Kara Sea (Arctic Ocean). *Geo-Marine Lett.* **2007**. [[CrossRef](#)]
36. Stein, R.; Fahl, K. The Laptev Sea: Distribution, Sources, Variability and Burial of Organic Carbon. In *The Organic Carbon Cycle in the Arctic Ocean*; Stein, R., Macdonald, R.W., Eds.; Springer: Berlin, Germany, 2004; pp. 213–237.
37. Stein, R.; Fahl, K. Holocene accumulation of organic carbon at the Laptev Sea continental margin (Arctic Ocean): Sources, pathways, and sinks. *Geo-Marine Lett.* **2000**, *20*, 27–36. [[CrossRef](#)]
38. Stein, R.; Fahl, K. The Kara Sea: Distribution, Sources, Variability and Burial of Organic Carbon. In *The Organic Carbon Cycle in the Arctic Ocean*; Stein, R., Macdonald, R.W., Eds.; Springer: Berlin, Germany, 2004; pp. 237–266.
39. Stapel, J.G.; Schirrmeister, L.; Overduin, P.P.; Wetterich, S.; Strauss, J.; Horsfield, B.; Mangelsdorf, K. Microbial lipid signatures and substrate potential of organic matter in permafrost deposits: Implications for future greenhouse gas production. *J. Geophys. Res. Biogeosci.* **2016**, *121*, 2652–2666. [[CrossRef](#)]
40. Stapel, J.G.; Schwamborn, G.; Schirrmeister, L.; Horsfield, B.; Mangelsdorf, K. Substrate potential of last interglacial to Holocene permafrost organic matter for future microbial greenhouse gas production. *Biogeosciences* **2018**, *15*, 1969–1985. [[CrossRef](#)]
41. Jakobsson, M.; Grantz, A.; Kristoffersen, Y.; Macnab, R.; MacDonald, R.W.; Sakshaug, E.; Stein, R.; Jokat, W. The Arctic Ocean: Boundary Conditions and Background Information. In *The Organic Carbon Cycle in the Arctic Ocean*; Springer: Berlin/Heidelberg, Germany, 2004; pp. 1–32.
42. Sakshaug, E. Primary and Secondary Production in the Arctic Seas. In *The Organic Carbon Cycle in the Arctic Ocean*; Springer: Berlin/Heidelberg, Germany, 2004; pp. 57–81.
43. Rachold, V.; Grigoriev, M.N.; Are, F.E.; Solomon, S.; Reimnitz, E.; Kassens, H.; Antonow, M. Coastal erosion vs riverline sediment discharge in the Arctic shelf seas. *Int. J. Earth Sci.* **2000**, *89*, 450–460. [[CrossRef](#)]
44. Semiletov, I.P.; Pipko, I.I.; Shakhova, N.E.; Dudarev, O.V.; Pugach, S.P.; Charkin, A.N.; McRoy, C.P.; Kosmach, D.; Gustafsson, Ö. Carbon transport by the Lena River from its headwaters to the Arctic Ocean, with emphasis on fluvial input of terrestrial particulate organic carbon vs. carbon transport by coastal erosion. *Biogeosciences* **2011**, *8*, 2407–2426. [[CrossRef](#)]
45. Holmes, R.M.; McClelland, J.W.; Peterson, B.J.; Tank, S.E.; Bulygina, E.; Eglinton, T.I.; Gordeev, V.V.; Gurtovaya, T.Y.; Raymond, P.A.; Repeta, D.J.; et al. Seasonal and Annual Fluxes of Nutrients and Organic Matter from Large Rivers to the Arctic Ocean and Surrounding Seas. *Estuaries Coasts* **2012**. [[CrossRef](#)]
46. Dudarev, O.V. Modern Lithomorphogenesis on the East Arctic Shelf. Ph.D. Thesis, Pacific Oceanological Institute, Far East Branch of Russian Academy of Sciences, Vladivostok, Russia. Tomsk Polytechnic University, Tomsk, Russia, 2016; p. 386.
47. Wegner, C.; Hölemann, J.A.; Dmitrenko, I.; Kirillov, S.; Kassens, H. Seasonal variations in Arctic sediment dynamics—Evidence from 1-year records in the Laptev Sea (Siberian Arctic). *Glob. Planet. Change* **2005**, *48*, 126–140. [[CrossRef](#)]
48. Eicken, H.; Reimnitz, E.; Alexandrov, V.; Martin, T.; Kassens, H.; Viehoff, T. Sea-ice processes in the Laptev Sea and their importance for sediment export. *Cont. Shelf Res.* **1997**. [[CrossRef](#)]
49. Reimnitz, E.; Dethleff, D.; Nürnberg, D. Contrasts in Arctic shelf sea-ice regimes and some implications: Beaufort Sea versus Laptev Sea. *Mar. Geol.* **1994**, *119*, 215–225. [[CrossRef](#)]
50. Folk, R.L.; Ward, W.C. Brazos River bar [Texas]; a study in the significance of grain size parameters. *J. Sediment. Res.* **1957**, *27*, 3–26. [[CrossRef](#)]
51. Baudin, F.; Disnar, J.-R.; Aboussou, A.; Savignac, F. Guidelines for Rock-Eval analysis of recent marine sediments. *Org. Geochem.* **2015**, *86*, 71–80. [[CrossRef](#)]
52. Carrie, J.; Sanei, H.; Stern, G. Standardisation of Rock-Eval pyrolysis for the analysis of recent sediments and soils. *Org. Geochem.* **2012**, *46*, 38–53. [[CrossRef](#)]
53. Gershelis, E.V.; Kashapov, R.S.; Ruban, A.S.; Oberemok, I.A.; Leonov, A.A.; Chernykh, D.V.; Dudarev, O.V.; Semiletov, I.P. Identifying sources of organic carbon in surface sediments of laptev sea shelf using a rock-eval approach. *Bull. Tomsk Polytech. Univ. Geo Assets Eng.* **2020**, *331*, 189–198. [[CrossRef](#)]

54. Dethleff, D.; Kuhlmann, G. Fram Strait sea-ice sediment provinces based on silt and clay compositions identify Siberian Kara and Laptev seas as main source regions. *Polar Res.* **2010**, *29*, 265–282. [[CrossRef](#)]
55. Panova, E.V.; Ruban, A.S.; Dudarev, O.V.; Tesi, T.; Broöder, L.; Gustafsson, O.; Grinko, A.A.; Shakhova, N.E.; Goncharov, I.V.; Mazurov, A.K.; et al. Lithological features of surface sediment and their influence on organic matter distribution across the east-Siberian Arctic shelf. *Bull. Tomsk Polytech. Univ. Geo Assets Eng.* **2017**, *328*, 94–105.
56. Shakhova, N.; Semiletov, I.; Sergienko, V.; Lobkovsky, L.; Yusupov, V.; Salyuk, A.; Salomatin, A.; Chernykh, D.; Kosmach, D.; Panteleev, G.; et al. The East Siberian Arctic Shelf: Towards further assessment of permafrost-related methane fluxes and role of sea ice. *Philos. Trans. R. Soc. A Math. Phys. Eng. Sci.* **2015**, *373*, 20140451. [[CrossRef](#)]
57. Shakhova, N.; Semiletov, I.; Leifer, I.; Sergienko, V.; Salyuk, A.; Kosmach, D.; Chernykh, D.; Stubbs, C.; Nicolsky, D.; Tumskey, V.; et al. Ebullition and storm-induced methane release from the East Siberian Arctic Shelf. *Nat. Geosci.* **2014**, *7*, 64–70. [[CrossRef](#)]
58. Shakhova, N.; Semiletov, I.; Gustafsson, O.; Sergienko, V.; Lobkovsky, L.; Dudarev, O.; Tumskey, V.; Grigoriev, M.; Mazurov, A.K.; Salyuk, A.; et al. Current rates and mechanisms of subsea permafrost degradation in the East Siberian Arctic Shelf. *Nat. Commun.* **2017**, *8*, 1–13. [[CrossRef](#)]
59. Jakobsson, M. Submarine glacial landform distribution in the central Arctic Ocean shelf-slope-basin system. *Geol. Soc. Mem.* **2016**, *46*, 469–476. [[CrossRef](#)]
60. Lobkovsky, L.I.; Nikiforov, S.L.; Ananiev, R.A.; Khortov, A.V.; Semiletov, I.P.; Jakobsson, M.; Dmitrievskiy, N.N. Recent geological–geomorphological processes on the east Arctic shelf: Results of the expedition of the icebreaker Oden in 2014. *Oceanology* **2015**, *55*, 926–929. [[CrossRef](#)]
61. Barnes, P.W.; Asbury, J.L.; Rearic, D.M.; Ross, C.R. Ice erosion of a sea-floor knickpoint at the inner edge of the stamukhi zone, Beaufort Sea, Alaska. *Mar. Geol.* **1987**, *76*, 207–222. [[CrossRef](#)]
62. Jakobsson, M.; Nilsson, J.; Anderson, L.; Backman, J.; Björk, G.; Cronin, T.M.; Kirchner, N.; Koshurnikov, A.; Mayer, L.; Noormets, R.; et al. Evidence for an ice shelf covering the central Arctic Ocean during the penultimate glaciation. *Nat. Commun.* **2016**, *7*. [[CrossRef](#)]
63. Ananyev, R.; Dmitrievskiy, N.; Jakobsson, M.; Lobkovsky, L.; Nikiforov, S.; Roslyakov, A.; Semiletov, I. Sea-ice ploughmarks in the eastern Laptev Sea, East Siberian Arctic shelf. *Geol. Soc. Mem.* **2016**, *46*, 301–302. [[CrossRef](#)]
64. O'Regan, M.; Backman, J.; Barrientos, N.; Cronin, T.M.; Gemery, L.; Kirchner, N.; Mayer, L.A.; Nilsson, J.; Noormets, R.; Pearce, C.; et al. The De Long Trough: A newly discovered glacial trough on the East Siberian continental margin. *Clim. Past* **2017**, *13*, 1269–1284. [[CrossRef](#)]
65. Stein, R.; Macdonald, R.W. References. In *The Organic Carbon Cycle in the Arctic Ocean*; Springer: Berlin/Heidelberg, Germany, 2004; pp. 323–363.
66. Schirrmeister, L.; Dietze, E.; Matthes, H.; Grosse, G.; Strauss, J.; Laboor, S.; Ulrich, M.; Kienast, F.; Wetterich, S. The genesis of Yedoma Ice Complex permafrost-grain-size endmember modeling analysis from Siberia and Alaska. *E&G Quat. Sci. J* **2020**, *69*, 33–53. [[CrossRef](#)]
67. Strauss, J.; Schirrmeister, L.; Wetterich, S.; Borchers, A.; Davydov, S.P. Grain-size properties and organic-carbon stock of Yedoma Ice Complex permafrost from the Kolyma lowland, northeastern Siberia. *Glob. Biogeochem. Cycles* **2012**, *26*. [[CrossRef](#)]
68. Grigoriev, M.N.; Razumov, S.O.; Kunitzky, V.V.; and Spektor, V.B. Dinamika beregov vostochnykh arkticheskikh morey Rossii: Osnovnye faktory, zakonomernosti i tendencii (Dynamics of the Russian East Arctic Sea coast: Major factors, regularities and tendencies). *Kriosf. Zemli (Earth's Cryosphere)* **2006**, *10*, 74–94.
69. Dethleff, D. Dense water formation in the Laptev Sea flaw lead. *J. Geophys. Res. Ocean.* **2010**, *115*. [[CrossRef](#)]
70. Stein, R.; Macdonald, R.W. Organic Carbon Budget: Arctic Ocean vs. Global Ocean. In *The Organic Carbon Cycle in the Arctic Ocean*; Springer: Berlin/Heidelberg, Germany, 2004; pp. 315–322.
71. Gustafsson, Ö.; Van Dongen, B.E.; Vonk, J.E.; Dudarev, O.V.; Semiletov, I.P. Widespread release of old carbon across the Siberian Arctic echoed by its large rivers. *Biogeosciences* **2011**, *8*, 1737–1743. [[CrossRef](#)]
72. Bergamaschi, B.A.; Tsamakidis, E.; Keil, R.G.; Eglinton, T.I.; Montluçon, D.B.; Hedges, J.I. The effect of grain size and surface area on organic matter, lignin and carbohydrate concentration, and molecular compositions in Peru Margin sediments. *Geochim. Cosmochim. Acta* **1997**, *61*, 1247–1260. [[CrossRef](#)]

73. Mayer, L.M. Surface area control of organic carbon accumulation in continental shelf sediments. *Geochim. Cosmochim. Acta* **1994**. [[CrossRef](#)]
74. Mayer, L.M. Relationships between mineral surfaces and organic carbon concentrations in soils and sediments. *Chem. Geol.* **1994**. [[CrossRef](#)]
75. Disnar, J.R.; Guillet, B.; Keravis, D.; Di-Giovanni, C.; Sebag, D. Soil organic matter (SOM) characterization by Rock-Eval pyrolysis: Scope and limitations. *Org. Geochem.* **2003**, *34*, 327–343. [[CrossRef](#)]
76. Zimov, S.A.; Schuur, E.A.G.; Stuart Chapin, F. Permafrost and the global carbon budget. *Science* **2006**, *312*, 1612–1613. [[CrossRef](#)]
77. Hedges, J.I.; Cowie, G.L.; Richey, J.E.; Quay, P.D.; Benner, R.; Strom, M.; Forsberg, B.R. Origins and processing of organic matter in the Amazon River as indicated by carbohydrates and amino acids. *Limnol. Oceanogr.* **1994**, *39*, 743–761. [[CrossRef](#)]
78. Bröder, L.; Tesi, T.; Andersson, A.; Semiletov, I.; Gustafsson, Ö. Bounding cross-shelf transport time and degradation in Siberian-Arctic land-ocean carbon transfer. *Nat. Commun.* **2018**. [[CrossRef](#)]
79. Salvadó, J.A.; Tesi, T.; Sundbom, M.; Karlsson, E.; Kruså, M.; Semiletov, I.P.; Panova, E.; Gustafsson, Ö. Contrasting composition of terrigenous organic matter in the dissolved, particulate and sedimentary organic carbon pools on the outer East Siberian Arctic Shelf. *Biogeosciences* **2016**, *13*. [[CrossRef](#)]
80. Hedges, J.I.; Blanchette, R.A.; Weliky, K.; Devol, A.H. Effects of fungal degradation on the CuO oxidation products of lignin: A controlled laboratory study. *Geochim. Cosmochim. Acta* **1988**, *52*, 2717–2726. [[CrossRef](#)]
81. Hicks, R.E.; Owen, C.J.; Aas, P. Deposition, resuspension, and decomposition of particulate organic matter in the sediments of Lake Itasca, Minnesota, USA. *Hydrobiologia* **1994**, *284*, 79–91. [[CrossRef](#)]
82. Meyers, P.A.; Ishiwatari, R. Lacustrine organic geochemistry—an overview of indicators of organic matter sources and diagenesis in lake sediments. *Org. Geochem.* **1993**, *20*, 867–900. [[CrossRef](#)]
83. Eglinton, G.; Hamilton, R.J. Leaf epicuticular waxes. *Science* **1967**, *156*, 1322–1335. [[CrossRef](#)]
84. Vonk, J.E.; Van Dongen, B.E.; Gustafsson, Ö. Selective preservation of old organic carbon fluvially released from sub-Arctic soils. *Geophys. Res. Lett.* **2010**, *37*, L11605. [[CrossRef](#)]
85. Feng, X.; Gustafsson, R.M.; Vonk, J.E.; Van Dongen, B.E.; Semiletov, I.P.; Dudarev, O.V.; Yunker, M.B.; MacDonald, R.W.; Montluçon, D.B.; et al. Multi-molecular tracers of terrestrial carbon transfer across the pan-Arctic: Comparison of hydrolyzable components with plant wax lipids and lignin phenols. *Biogeosciences* **2015**, *12*, 4841–4860. [[CrossRef](#)]
86. Bray, E.E.; Evans, E.D. Distribution of n-paraffins as a clue to recognition of source beds. *Geochim. Cosmochim. Acta* **1961**, *22*, 2–15. [[CrossRef](#)]
87. Marzi, R.; Torkelson, B.E.; Olson, R.K. A revised carbon preference index. *Org. Geochem.* **1993**, *20*, 1303–1306. [[CrossRef](#)]
88. Peters, K.E.; Walters, C.C.; Moldowan, J.M. *The Biomarker Guide, Biomarkers and Isotopes in Petroleum Exploration and Earth History*; Cambridge University Press: Cambridge, UK, 2005.

**Publisher’s Note:** MDPI stays neutral with regard to jurisdictional claims in published maps and institutional affiliations.



© 2020 by the authors. Licensee MDPI, Basel, Switzerland. This article is an open access article distributed under the terms and conditions of the Creative Commons Attribution (CC BY) license (<http://creativecommons.org/licenses/by/4.0/>).